From the Phan-Thien Tanner / Oldroyd-B non-Newtonian model to the double shear thining Rabinowisch thin film model

Guy Bayada, Laurent Chupin, Sébastien Martin

From the Phan-Thien Tanner / Oldroyd-B non-Newtonian model to the double shear thining Rabinowisch thin film model

Guy Bayada
Université de Lyon,
INSA-Lyon, Institut Camille Jordan (CNRS UMR 5208)
& LaMCoS (CNRS UMR 5514),
Bât. Léonard de Vinci, 21 avenue Jean Capelle,
F-69621 Villeurbanne cedex, France.
Email: guy.bayada@insa-lyon.fr

Laurent Chupin
Université Blaise Pascal, Clermont-Ferrand II,
Laboratoire de Mathématiques, CNRS-UMR 6620,
Campus des Cézeaux,
F-63177 Aubière cedex, France.
Email: laurent.chupin@math.univ-bpclermont.fr

Sébastien Martin
Université Paris-Sud 11,
Laboratoire de Mathématiques, CNRS-UMR 8628,
Bâtiment 425 (Mathématique),
F-91405 Orsay cedex, France.
Email: sebastien.martin@math.u-psud.fr

ABSTRACT

In this paper, an asymptotic expansion is used to derive a description of Phan-Tien Tanner / Oldroyd-B flows in the thin film situation without the classical "Upper Convective Maxwell" assumption. We begin with a short presentation of the Phan-Thien Tanner / Oldroyd-B models which introduce viscoelastic effects in a solute-solvant mixture. The three dimensional flow is described using five parameters, namely De *the Deborah number (or the relaxation parameter* λ*), the viscosity ratio r, the bulk fluid viscosity* η*, the material slip parameter a related to the "convected derivative" and an elongation number* κ*. Then we focus on the thin film assumption and the related asymptotic analysis that allows us to derive a reduced model. A perturbation procedure for "not too small" values of* κ *allows us to obtain further results such as an asymptotic "effective viscosity / shear rate" law which appears to be a perturbation of the double Rabinowisch model whose parameters are completely defined by those of the original three dimensional model. And last a numerical procedure is proposed based on a penalized Uzawa method, to compute the corresponding solution. This algorithm can also be used for any generalized double Newtonian shear thinning Carreau law.*

Nomenclature

$\mathcal{H}$ Order of magnitude of the gap
$\mathcal{L}$ Order of magnitude of the bearing length
$\mathcal{U}$ Order of magnitude of the shear velocity
L_1, L_2 Dimensions of the contact area
H (h) Gap (dimensionless)
$\varepsilon = \mathcal{H}/\mathcal{L}$ Film thickness ratio
Re Reynolds number
De ($\widetilde{\mathrm{De}} = \mathrm{De}/\varepsilon$) Deborah number (rescaled)
κ ($\mathrm{K} = \kappa/r$, $\widetilde{\mathrm{K}} = \mathrm{K}/\varepsilon$) Elongation number (rescaled)
b, c, n, G Parameters in Carreau-Yosida law
a Material slip parameter in the time derivative
r Ratio of viscosities or retardation number
λ Relaxation time
ρ Density
δ Convergence parameters in the algorithm
δ_{x_1}, δ_{x_2} Discretization parameters
s Dimensionless velocity at $z = 0$ in the direction x_1
$t^\star$ (t) Time (dimensionless)
$p^\star$ (p) Pressure (dimensionless)
q_0 Input mass flux value
$\mathbf{U}^\star = (u_1^\star, u_2^\star, w^\star)$ ($\mathbf{U} = (u_1, u_2, w)$) Velocity (dimensionless)
$\mathbf{x}^\star = (x_1^\star, x_2^\star)$, ($\mathbf{x} = (x_1, x_2)$) Coordinates on the shearing surface (dimensionless)
$z^\star$ (z) Orthogonal coordinate (dimensionless)
$D(\mathbf{U}) = \frac{1}{2}\left(\nabla\mathbf{U} + {}^T(\nabla\mathbf{U})\right)$ Symmetric parts of the velocity gradient
$W(\mathbf{U}) = \frac{1}{2}\left(\nabla\mathbf{U} - {}^T(\nabla\mathbf{U})\right)$ Skew-symmetric parts of the velocity gradient
$\dot{\gamma}$ ($\dot{\alpha}$, $\dot{\beta}$) Shear rate (dimensionless 1D -for long devices- or 2D)
η_1, η_2, $\eta_{\mathrm{el.}}$, $\eta_{\mathrm{visc.}}$, η_{eff}, η Viscosities
$\sigma^\star$, $\sigma_{\mathrm{el.}}^\star$, $\sigma_{\mathrm{visc.}}^\star$ (σ, $\sigma_{\mathrm{el.}}$, $\sigma_{\mathrm{visc.}}$) Stress tensor (dimensionless)
τ Shear stress
ω Contact area

1 Introduction

Many authors have investigated the non-Newtonian effects of fluids based upon various rheological models in lubrication [1]. In most of them, the main keypoint relies on the choice of the relationship between the effective viscosity η_{eff} and the shear rate $\dot{\gamma}$ (or the effective viscosity η_{eff} and the shear stress τ). For mineral oil / polymer blends this relation shows a shear thinning effect (decreasing slope) of the power law type and two plateaux (corresponding to either small stress values or high stress values). This behavior is known as double Newtonian shear thinning. As for full 3D non-Newtonian Navier-Stokes fluids [2, 3] Carreau-Yasuda models are often used:

$$\eta_{\mathrm{eff}}(\dot{\gamma}) = \eta_2 + \frac{\eta_1 - \eta_2}{\left(1 + \left(b\dot{\gamma}\right)^c\right)^{\frac{1-n}{c}}} \quad \text{or} \quad \eta_{\mathrm{eff}}(\tau) = \eta_2 + \frac{\eta_1 - \eta_2}{\left(1 + \left(\tau/G\right)^c\right)^{\frac{1-n}{c}}} \tag{1}$$

Values of the parameters are often obtained by fitting experimental data [4–8] although specific values are sometimes obtained using ad-hoc physical reasons (like $c = 2/3$, $n = 1/3$ for pseudo-plastic systems in Cross [9]). It has been also observed that some values of the parameters allow us to obtain a one dimensional Reynolds equation (Ellis model: $\eta_2 = 0$, $c = 1 - n$ in [10], double Rabinowisch model, $c = 2$, $n = -1$ in [4], double Ferry model $c = 1$, $n = 0$ [4], approximate single Carreau model $\eta_2 = 0$, $c = 2$ in [11], single Rabinowisch model in [12]), or even two dimensional Reynolds equation with the single Rabinowisch model [6, 13]. However, only two of them are able to deal with the double shear thinning feature. Let us mention also that a Reynolds-type equation is obtained for an Eyring fluid by T. F. Conry, S. Wang and C. Cusano [14]. The derivation of a generalized Reynolds equation is of particular interest as it prevents from performing additional integrations across the film, thus limiting computational costs. To deal with that difficulty, approximate 2D Reynolds equations have been sometimes proposed as in [15] and [16]. A comparison between these two approximations can be found in [17].

The present paper is concerned with another kind of results which are obtained by using asymptotic methods to derive reduced models based on the thin film assumption (with or without infinitely long devices assumption) starting from non-Newtonian Navier-Stokes models (depending on several rheological parameters: the fluid viscosity η, the retardation number r, the material slip parameter a, the elongation number κ, the fluid relaxation time λ which is directly related to the Deborah number De). Pioneering works are those of J. Tichy [18], and more recently F. T. Akyildiz and H. Bellout [19], and R. Zhang and X. K. Li [20]. In the work of J. Tichy [18], the departure point is the linear Maxwell purely elastic upper convective model (that corresponds to $r = 1$, $a = 1$, $\kappa = 0$, see Section 2 for the definition of those rheological parameters) and the Deborah number De is used as a perturbation parameter from the Newtonian pressure p_0 and velocity. In order to keep the greatest number of terms in the asymptotic equation (including non-Newtonian effects) and avoid singularity for small film thickness ratio ε, the scaling of the stress tensor is not the same for all the terms and De is of the same order of magnitude than ε which represents the film thickness ratio. Introducing pressure p_{De} corresponding to the viscoelastic configuration, and pressure p_0 corresponding to the Newtonian configuration, J. Tichy proposes an asymptotic expansion which takes the form (after dimensionless procedure) $p_{\mathrm{De}} = p_0 + \mathrm{De}\, p^{(c)}$, where $p^{(c)}$ is a corrective pressure obeying a Reynolds-type equation. In the work of F. T. Akyildiz and H. Bellout [19], the departure point is the Phan-Thien Tanner (PTT) / Maxwell model ($r = 1$, $a = 1$, $\kappa \neq 0$, see Section 2 for the definition of those rheological parameters). In order to balance the effects of the Newtonian and nonlinear contributions, it is assumed that the Deborah number and the stress tensor are also of the same order of magnitude as ε (thin film ratio). Collecting the leading terms of all the equations leads to the derivation of a new Reynolds equation. The difference with the results of J. Tichy is not only due to the nonlinearity in the stresses included in the PTT model, but also to the fact that the influence of De is now included in the obtained Reynolds equation. A close examination of these works show that the proposed asymptotic procedure is only valid under the assumption $a = 1$, corresponding to the so-called upper convective Maxwell (UCM) model. This choice allows easier computations but it is not relevant in some experiments or theoritical works, see for instance [21, 22] in which a value $a = 0.8$ is often retained. In that case the whole asymptotic procedure has to be revisited.

Section 2 is devoted to the presentation of the Phan-Thien Tanner / Oldroyd-B departure model. The asymptotic procedure is described in Sections 3 and 4. In both sections, as in [18, 19], the Deborah number De is of the same order of magnitude than the thin film ratio parameter. Unlike J. Tichy's assumption [18], dimensionless assumptions in our model are the same for all the components of the stress tensor. This has been rigorously proved in [23] for $\kappa = 0$ by G. Bayada, L. Chupin and B. Grec and the analysis is valid not only for 2D flows but also for 3D flows. Moreover we are able to cope with a wider range of material slip parameter values (which are related to the objective time derivates): more precisely, our work includes not only the classical Jaumann one ($a = 0$) but also any value between lower convected derivatives ($a = -1$) and upper convective derivatives ($a = 1$). Similarly, any combination of viscous and elastic effects can be obtained by defining a retardation parameter value (denoted r) between 0 and 1.

In Section 3, the elongation number κ is assumed to be very small (same order of the magnitude of ε) and consequently disappears in the asymptotic procedure. The resulting constitutive equation reads:

$$\eta_{\mathrm{eff}} = \eta_2 + \frac{\eta_1 - \eta_2}{1 + \left(b\dot{\gamma}\right)^2} \tag{2}$$

All parameters can be linked with those of the 3D model by:

$$b = \lambda\sqrt{1-a^2}, \qquad \eta_2 = (1-r)\,\eta \quad \text{and} \quad \eta_1 = \eta,$$

where viscosity η can be related to the viscous or elastic contributions of the fluid (see Eq. (10)). Equation (2), together with the asymptotic hydrodynamic mass flow equation allows us to compute all the characteristics of the flow.

In Section 4, we aim at introducing the elongation effects in the anisotropic law. To do so, we pick out the same scaling for the Deborah number and the stress tensor while κ is assumed to be of order zero with respect to the aspect ratio. The nonlinear asymptotic system is solved for small values of κ by using a perturbation procedure as in [18, 20]. The constitutive equation can be written as

$$\eta_{\mathrm{eff}} = \eta_2 + \frac{\eta_1 - \eta_2}{1 + \left(b\dot{\gamma}\right)^2} + \kappa g(a, r, \lambda, \dot{\gamma}). \tag{3}$$

Numerical results appear in Section 5. In a first simulation, for a non-Newtonian configuration, effective viscosity and stresses distributions are computed, revealing in particular heterogeneity of the effective viscosity in the 3D flow. Then we

focus on the influence of the elongation number on the viscoelastic flow. We also discuss the influence of the Deborah number De: it is proved that the difference between the non-Newtonian pressure and the Newtonian one is proportional to De^2 and not to De as for the UCM model proposed in [18]. We finally provide some information on the way the load does depend on the rheological properties of the fluid. Additional results are presented in the Appendices: supplementary results about the influence of rheological parameters appear in Appendix A. It is observed in Appendix B that the classical infinitely long bearing assumption may be irrelevant due to the non-Newtonian effects, at least in some particular cases of oil supply. At last a new algorithm is proposed in Appendix C to solve the non Newtonian problem: the idea is to introduce a fixed point procedure and a penalization of the divergence free equation which acts as an implicit Reynolds equation. This procedure is based on separate computations in the directions of the flow and in the direction normal to the flow. Let us remark that it can be easily parallelized and deal with other laws that differ from the Rabinowisch one. We can get both pressure and velocity for various values of the parameters a, $\widetilde{\mathrm{De}}$ and r as well as the classical geometrical characteristics.

2 Phan-Thien Tanner (PTT) / Oldroyd-B model

The Phan-Thien Tanner / Oldroyd-B model is one of the most used models, which is able to describe viscoelastic flows for mixtures, see [19, 24]. It is based on a constitutive equation which is an interpolation between purely viscous and purely elastic behaviors.

The constitutive equation for the elastic part of the fluid obeys the Phan-Thien Tanner law:

$$\lambda\left(\frac{\partial\sigma^\star_{\mathrm{el.}}}{\partial t^\star}+\mathbf{U}^\star\cdot\nabla\sigma^\star_{\mathrm{el.}}+g_a(\nabla\mathbf{U}^\star,\sigma^\star_{\mathrm{el.}})\right)+f(\sigma^\star_{\mathrm{el.}})\,\sigma^\star_{\mathrm{el.}}=2\eta_{\mathrm{el.}}D(\mathbf{U}^\star), \tag{4}$$

in which $\eta_{\mathrm{el.}}$ and λ are positive constants which respectively correspond to the fluid viscosity and the relaxation time. The vector field $\mathbf{U}^\star=(u_1^\star,u_2^\star,w^\star)$ is the lubricant velocity, $p^\star$ the pressure and $\sigma^\star_{el.}$ the extra-stress symmetric tensor. Function f will be defined later. The bilinear application g_a, $-1\le a\le 1$, is defined by

$$g_a(\nabla\mathbf{U}^\star,\sigma^\star_{\mathrm{el.}})=\sigma^\star_{\mathrm{el.}}\cdot W(\mathbf{U}^\star)-W(\mathbf{U}^\star)\cdot\sigma^\star_{\mathrm{el.}}-a\left(\sigma^\star_{\mathrm{el.}}\cdot D(\mathbf{U}^\star)+D(\mathbf{U}^\star)\cdot\sigma^\star_{\mathrm{el.}}\right) \tag{5}$$

where $D(\mathbf{U}^\star)$ and $W(\mathbf{U}^\star)$ are respectively the symmetric and skew-symmetric parts of the velocity gradient $\nabla\mathbf{U}^\star$. Usually, $D(\mathbf{U}^\star)$ is called the rate of strain tensor and $W(\mathbf{U}^\star)$ is called the vorticity tensor. Notice that the parameter a is considered as a dimensionless material slip parameter which interpolates between upper convected ($a=1$) and lower convective derivatives ($a=-1$), the case $a=0$ being the corotational case [25]. Finally, a usual choice for the function f gives the PTT model (see [19, 24]):

$$f(\sigma^\star_{\mathrm{el.}})=1+\frac{\kappa\lambda}{\eta_{\mathrm{el.}}}\mathrm{Tr}(\sigma^\star_{\mathrm{el.}}), \tag{6}$$

in which κ is a parameter related to the elongational behavior of the model. Notice also that the simple case $f\equiv 1$ provides the Oldroyd-B model.

A Newtonian fluid obeys the classical law:

$$\sigma^\star_{\mathrm{visc.}}=2\eta_{\mathrm{visc.}}D(\mathbf{U}^\star), \tag{7}$$

where $\eta_{\mathrm{visc.}}$ corresponds to the Newtonian viscosity (often associated with a solvent).

The behaviour of a viscoelastic fluid is given by the balance of momentum equation, which reads (without body forces) by introducing pressure $p^\star$:

$$\rho\left(\frac{\partial\mathbf{U}^\star}{\partial t^\star}+\mathbf{U}^\star\cdot\nabla\mathbf{U}^\star\right)+\nabla p^\star=\ \mathrm{div}\ (\sigma^\star_{\mathrm{visc.}}+\sigma^\star_{\mathrm{el.}}), \tag{8}$$

where ρ is the mass density of the fluid. It can be rewritten as:

$$\rho\left(\frac{\partial \mathbf{U}^\star}{\partial t^\star} + \mathbf{U}^\star \cdot \nabla \mathbf{U}^\star\right) + \nabla p^\star - \eta_{\text{visc.}} \Delta \mathbf{U}^\star - \text{ div } \sigma^\star_{\text{el.}} = \mathbf{0}. \tag{9}$$

It is usual in the Oldroyd-B model to introduce two new parameters: a total viscosity number η and a retardation parameter r instead of $\eta_{\text{visc.}}$ and $\eta_{\text{el.}}$ such that

$$\eta = \eta_{\text{visc.}} + \eta_{\text{el.}} \quad \text{and} \quad r = \frac{\eta_{\text{el.}}}{\eta_{\text{visc.}} + \eta_{\text{el.}}}. \tag{10}$$

Using the incompressibility assumption, the overall system of equation is written as

$$\rho\left(\frac{\partial \mathbf{U}^\star}{\partial t^\star} + \mathbf{U}^\star \cdot \nabla \mathbf{U}^\star\right) - \eta(1-r)\Delta \mathbf{U}^\star + \nabla p^\star - \text{ div } \sigma^\star_{\text{el.}} = \mathbf{0}, \tag{11}$$

$$\text{div } \mathbf{U}^\star = 0, \tag{12}$$

$$\lambda\left(\frac{\partial \sigma^\star_{\text{el.}}}{\partial t^\star} + \mathbf{U}^\star \cdot \nabla \sigma^\star_{\text{el.}} + g_a(\nabla \mathbf{U}^\star, \sigma^\star_{\text{el.}})\right) + f(\sigma^\star_{\text{el.}})\, \sigma^\star_{\text{el.}} = 2\eta r D(\mathbf{U}^\star). \tag{13}$$

Choosing $\kappa = 0$ and $r = 1$ provides the classical Maxwell model.

3 Asymptotic analysis of the thin film flow equations for very small elongation numbers

The space coordinates are denoted by $(x_1^\star, x_2^\star, z^\star)$ or more simply by $(\mathbf{x}^\star, z^\star)$ with $\mathbf{x}^\star = (x_1^\star, x_2^\star)$. Let ω be a fixed bounded domain of the plane $z^\star = 0$. The upper surface of the gap is defined by $z^\star = H(\mathbf{x}^\star)$ (see Fig. 1)

By introducing characteristic lengths $\mathcal{L}$ for the domain ω and $\mathcal{H}$ for the size of the gap, we can define the film thickness ratio, the usual Deborah number and an elongation number

$$\varepsilon = \frac{\mathcal{H}}{\mathcal{L}}, \quad \text{De} = \frac{\lambda \mathcal{U}}{\mathcal{L}} \quad \text{and} \quad \text{K} = \frac{\kappa}{r}. \tag{14}$$

The governing equations, Eqs. (11)–(13), can be expressed in dimensionless form in terms of the following dimensionless quantities :

$$\mathbf{x} = \frac{\mathbf{x}^\star}{\mathcal{L}}, \quad z = \frac{z^\star}{\varepsilon \mathcal{L}}, \quad u_i = \frac{u_i^\star}{\mathcal{U}}, \quad w = \frac{w^\star}{\varepsilon \mathcal{U}}, \tag{15}$$

$$p = p^\star \frac{\varepsilon^2 \mathcal{L}}{\eta\, \mathcal{U}}, \quad \sigma = \sigma^\star_{\text{el.}} \frac{\varepsilon \mathcal{L}}{\eta\, \mathcal{U}}, \quad t = t^\star \frac{\mathcal{U}}{\mathcal{L}}. \tag{16}$$

We now rescale the three classical numbers: the Reynolds number which characterises the viscous forces compared to the convective ones, the Deborah number which highlights the elasticity of the fluid and the elongation number. Let us introduce:

$$\text{Re} = \frac{\rho \mathcal{U} \mathcal{L}}{\eta}, \quad \widetilde{\text{De}} = \frac{\text{De}}{\varepsilon} \quad \text{and} \quad \widetilde{\text{K}} = \frac{\text{K}}{\varepsilon}. \tag{17}$$

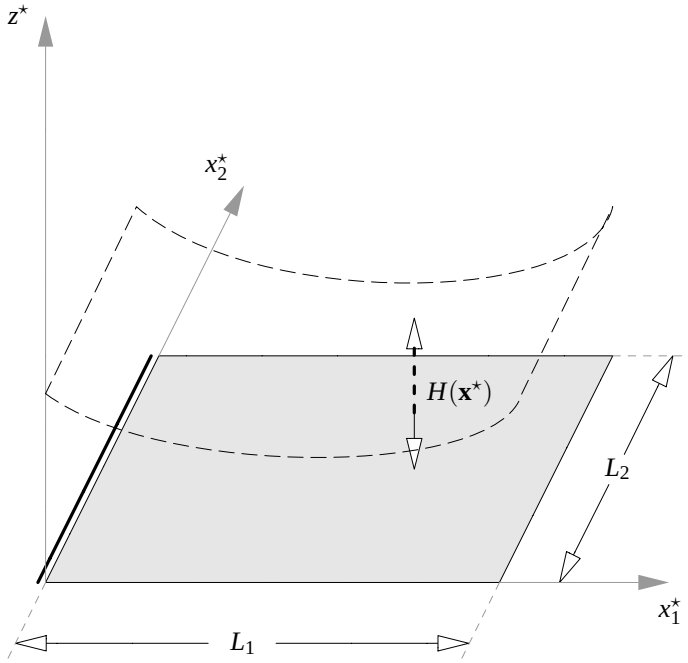

Fig. 1. Physical domain

For convenience, we also introduce the normalized gap function:

$$h(\mathbf{x}) = \frac{H(\mathbf{x}^\star)}{\varepsilon \mathcal{L}}. \tag{18}$$

In all this section, as suggested by the title of the section, K is assumed to be very small, i. e. K is of order ε (or less). The length and velocity scaling, see Eq. (15), takes into account the thin film nature of lubricant flow. Scalings related to Re, $\widetilde{\mathrm{De}}$ and $\widetilde{\mathrm{K}}$ can be viewed as assumptions related to operating conditions for which the present study is valid: Re and $\widetilde{\mathrm{De}}$ must be of order zero with respect to ε. As discussed in the introduction, the scaling on the pressure and the shear rate is based upon balancing principles that put forth the leading terms and can be rigorously proven to be valid (see [23]). By substituting these dimensionless variables, see Eqs. (15)–(17), into Eqs. (11)–(13), we obtain the dimensionless governing equations.

The three components of the momentum equation, namely Eq. (11), are written (the notation $\mathrm{d}/\mathrm{d}t$ denotes the convective derivative):

$$\begin{cases} \mathrm{Re}\dfrac{\mathrm{d}u_1}{\mathrm{d}t} - (1-r)\left(\dfrac{\partial^2 u_1}{\partial x_1^2} + \dfrac{\partial^2 u_1}{\partial x_2^2} + \dfrac{1}{\varepsilon^2}\dfrac{\partial^2 u_1}{\partial z^2}\right) + \dfrac{1}{\varepsilon^2}\dfrac{\partial p}{\partial x_1} \\ \qquad\qquad -\dfrac{1}{\varepsilon}\left(\dfrac{\partial \sigma_{1,1}}{\partial x_1} + \dfrac{\partial \sigma_{1,2}}{\partial x_2} + \dfrac{1}{\varepsilon}\dfrac{\partial \sigma_{1,3}}{\partial z}\right) = 0, \\ \mathrm{Re}\dfrac{\mathrm{d}u_2}{\mathrm{d}t} - (1-r)\left(\dfrac{\partial^2 u_2}{\partial x_1^2} + \dfrac{\partial^2 u_2}{\partial x_2^2} + \dfrac{1}{\varepsilon^2}\dfrac{\partial^2 u_2}{\partial z^2}\right) + \dfrac{1}{\varepsilon^2}\dfrac{\partial p}{\partial x_2} \\ \qquad\qquad -\dfrac{1}{\varepsilon}\left(\dfrac{\partial \sigma_{1,2}}{\partial x_1} + \dfrac{\partial \sigma_{2,2}}{\partial x_2} + \dfrac{1}{\varepsilon}\dfrac{\partial \sigma_{2,3}}{\partial z}\right) = 0, \\ \varepsilon\mathrm{Re}\dfrac{\mathrm{d}w}{\mathrm{d}t} - \varepsilon(1-r)\left(\dfrac{\partial^2 w}{\partial x_1^2} + \dfrac{\partial^2 w}{\partial x_2^2} + \dfrac{1}{\varepsilon^2}\dfrac{\partial^2 w}{\partial z^2}\right) + \dfrac{1}{\varepsilon^3}\dfrac{\partial p}{\partial z} \\ \qquad\qquad -\dfrac{1}{\varepsilon}\left(\dfrac{\partial \sigma_{1,3}}{\partial x_1} + \dfrac{\partial \sigma_{2,3}}{\partial x_2} + \dfrac{1}{\varepsilon}\dfrac{\partial \sigma_{3,3}}{\partial z}\right) = 0. \end{cases}$$

For small ε, these equations formally reduce to the following set of equations:

$$\begin{cases} -(1-r)\dfrac{\partial^2 u_1}{\partial z^2} + \dfrac{\partial p}{\partial x_1} - \dfrac{\partial \sigma_{1,3}}{\partial z} = 0, \\ -(1-r)\dfrac{\partial^2 u_2}{\partial z^2} + \dfrac{\partial p}{\partial x_2} - \dfrac{\partial \sigma_{2,3}}{\partial z} = 0, \\ \dfrac{\partial p}{\partial z} = 0, \end{cases} \tag{19}$$

Due to the previous dimensionless procedure the free divergence condition is preserved for the dimensionless variables:

$$\frac{\partial u_1}{\partial x_1} + \frac{\partial u_2}{\partial x_2} + \frac{\partial w}{\partial z} = 0, \tag{20}$$

Concerning the constitutive law, the process is similar: equations are written for the dimensionless quantities, then, passing formally to the limit $\varepsilon \to 0$, the following equations are obtained:

$$\begin{cases} \sigma_{1,1} + \widetilde{\mathrm{De}}(1-a)\sigma_{1,3}\dfrac{\partial u_1}{\partial z} = 0, \\ \sigma_{2,2} + \widetilde{\mathrm{De}}(1-a)\sigma_{2,3}\dfrac{\partial u_2}{\partial z} = 0, \\ \sigma_{3,3} - \widetilde{\mathrm{De}}(1+a)(\sigma_{1,3}\dfrac{\partial u_1}{\partial z} + \sigma_{2,3}\dfrac{\partial u_2}{\partial z}) = 0, \\ \sigma_{1,2} + \dfrac{\widetilde{\mathrm{De}}}{2}(1-a)(\sigma_{2,3}\dfrac{\partial u_1}{\partial z} + \sigma_{1,3}\dfrac{\partial u_2}{\partial z}) = 0, \\ \sigma_{1,3} + \dfrac{\widetilde{\mathrm{De}}}{2}\left((1-a)\sigma_{3,3}\dfrac{\partial u_1}{\partial z} - (1+a)\sigma_{1,2}\dfrac{\partial u_2}{\partial z} - (1+a)\sigma_{1,1}\dfrac{\partial u_1}{\partial z}\right) = r\dfrac{\partial u_1}{\partial z}, \\ \sigma_{2,3} + \dfrac{\widetilde{\mathrm{De}}}{2}\left((1-a)\sigma_{3,3}\dfrac{\partial u_2}{\partial z} - (1+a)\sigma_{1,2}\dfrac{\partial u_1}{\partial z} - (1+a)\sigma_{2,2}\dfrac{\partial u_2}{\partial z}\right) = r\dfrac{\partial u_2}{\partial z}. \end{cases} \tag{21}$$

As an example, we provide a full equation of the whole system before passing to the limit, namely the equation related to the first diagonal term in tensor σ:

$$\begin{aligned} \widetilde{\mathrm{De}}\Big\{\Big[\frac{\partial_t \sigma_{11}}{\partial t}\Big] + \Big[u_1\frac{\sigma_{11}}{\partial x_1} + u_2\frac{\sigma_{11}}{\partial x_2} + w\frac{\sigma_{11}}{\partial z}\Big] + \Big[\sigma_{12}\left(\frac{\partial u_1}{\partial x_2} - \frac{\partial u_2}{\partial x_1}\right) + \sigma_{13}\left(\frac{\partial u_1}{\varepsilon \partial z} - \varepsilon\frac{\partial w}{\partial x_1}\right)\Big] \\ -a\Big[2\sigma_{11}\frac{\partial u_1}{\partial x_1} + \sigma_{12}\left(\frac{\partial u_2}{\partial x_1} + \frac{\partial u_1}{\partial x_2}\right) + \sigma_{13}\left(\varepsilon\frac{\partial w}{\partial x_1} + \frac{\partial u_1}{\varepsilon \partial z}\right)\Big]\Big\} + \frac{\sigma_{11}}{\varepsilon} = 2r\frac{\partial u_1}{\partial x_1}, \end{aligned}$$

the asymptotic equation being obtained by considering the terms in ε^{-1}.

In this system, it is easy to see that coefficients $\sigma_{1,1}$, $\sigma_{2,2}$, $\sigma_{3,3}$ and $\sigma_{1,2}$ can be expressed as a function of $\sigma_{1,3}$, $\sigma_{2,3}$ and of the velocity (u_1, u_2). In addition, using the last two equations, $\sigma_{1,3}$ and $\sigma_{2,3}$ are expressed with respect to the velocity:

$$\begin{aligned} \sigma_{1,3} &= \frac{r\dfrac{\partial u_1}{\partial z}}{1 + \widetilde{\mathrm{De}}^2(1-a^2)\left(\left(\dfrac{\partial u_1}{\partial z}\right)^2 + \left(\dfrac{\partial u_2}{\partial z}\right)^2\right)}, \\ \sigma_{2,3} &= \frac{r\dfrac{\partial u_2}{\partial z}}{1 + \widetilde{\mathrm{De}}^2(1-a^2)\left(\left(\dfrac{\partial u_1}{\partial z}\right)^2 + \left(\dfrac{\partial u_2}{\partial z}\right)^2\right)}. \end{aligned}$$

For the sake of simplicity, let us denote by $\mathbf{u}$ the first two coordinates of the velocity vector: $\mathbf{u} = (u_1, u_2)$ and by G the following two components of the stress tensor: $\mathrm{G} = (\sigma_{1,3}, \sigma_{2,3})$. The system can be written in the following form:

$$\begin{cases} -(1-r)\dfrac{\partial^2 \mathbf{u}}{\partial z^2} - \dfrac{\partial \mathrm{G}}{\partial z} + \nabla_{\mathbf{x}} p = \mathbf{0}, \quad \text{with} \quad \mathrm{G} = \dfrac{r\dfrac{\partial \mathbf{u}}{\partial z}}{1 + \widetilde{\mathrm{De}}^2 (1-a^2) \left\| \dfrac{\partial \mathbf{u}}{\partial z} \right\|^2}, \\ \dfrac{\partial p}{\partial z} = 0, \\ \mathrm{div}_{\mathbf{x}} \mathbf{u} + \dfrac{\partial w}{\partial z} = 0, \end{cases} \tag{22}$$

all the other components of the stress tensor being directly deduced from Eq. (21).

Note that the first equation of Eqs. (22) also reads

$$\frac{\partial}{\partial z}\left(\eta_{\mathrm{eff}}^R \frac{\partial \mathbf{u}}{\partial z} \right) = \nabla_{\mathbf{x}} p, \tag{23}$$

with the (nonlinear) effective viscosity:

$$\eta_{\mathrm{eff}}^R (\mathbf{x}, z) = 1 - r + \frac{r}{1 + (1-a^2)\widetilde{\mathrm{De}}^2 \left\| \dfrac{\partial \mathbf{u}}{\partial z}(\mathbf{x}, z) \right\|^2}. \tag{24}$$

The vertical velocity w can be deduced from the horizontal velocity $\mathbf{u}$ by the free divergence condition. Coming back to the physical variables, we can check that Eqs. (22) can be rewritten

$$\begin{cases} \dfrac{\partial}{\partial z^\star}\left(\eta_{\mathrm{eff}} \dfrac{\partial \mathbf{u}^\star}{\partial z^\star} \right) = \nabla_{\mathbf{x}^\star} p^\star, \\ \dfrac{\partial p^\star}{\partial z^\star} = 0, \\ \mathrm{div}_{\mathbf{x}^\star}\left(\displaystyle\int_0^H \mathbf{u}^\star \, dz^\star \right) = w^\star(\cdot, 0) - w^\star(\cdot, H), \end{cases} \tag{25}$$

with

$$\eta_{\mathrm{eff}}(\dot\gamma) = \eta_{\mathrm{visc.}} + \frac{\eta_{\mathrm{el.}}}{1 + \lambda^2 (1-a^2) |\dot\gamma|^2}, \quad \text{and} \quad \dot\gamma = \left\| \frac{\partial \mathbf{u}^\star}{\partial z^\star} \right\| = \sqrt{\left(\frac{\partial u_1^\star}{\partial z^\star} \right)^2 + \left(\frac{\partial u_2^\star}{\partial z^\star} \right)^2}. \tag{26}$$

Let us remark that this model can lead to an ill-posed problem as long as the graph of function $\dot\gamma \mapsto \dot\gamma \eta_{\mathrm{eff}}(\dot\gamma)$ is not monotone. It can be proved (see [26]) that as long as $0 \leq r < 8/9$, Eqs. (25)–(26) have a unique solution. If $r \geq 8/9$, then existence or / and uniqueness may fail. Numerical experiments using the algorithm described in Appendix C show that non convergence situations appear as long as $r \geq 8/9$.

4 A perturbation method for small elongation numbers

The scaling used to obtain Eq. (21) is related to an elongation number K whose magnitude is assumed to be the same as the film thickness ratio ε. In that case this parameter does not contribute to the asymptotic problem. If K is of order zero with respect to ε, however small, it is possible to obtain an asymptotic problem in which the elongation number K does appear. For the sake of simplicity, computations will be led under the infinitely long assumption (i. e. with a 2D flow in the x_1-direction) although the method can be extended to a full 3D flow. Consequently, results will be also given in the 3D case, as a straightforward consequence of the previous analysis.

Under this assumption, when ε goes to zero, Eqs. (13) become:

$$\begin{cases} \mathrm{K}\widetilde{\mathrm{De}}\,\sigma_{1,1}(\sigma_{1,1}+\sigma_{3,3})+\sigma_{1,1}+\widetilde{\mathrm{De}}(1-a)\sigma_{1,3}\dfrac{\partial u_1}{\partial z}=0, \\ \mathrm{K}\widetilde{\mathrm{De}}\,\sigma_{3,3}(\sigma_{1,1}+\sigma_{3,3})+\sigma_{3,3}-\widetilde{\mathrm{De}}(1+a)\sigma_{1,3}\dfrac{\partial u_1}{\partial z}=0, \\ \mathrm{K}\widetilde{\mathrm{De}}\,\sigma_{1,3}(\sigma_{1,1}+\sigma_{3,3})+\sigma_{1,3}+\dfrac{\widetilde{\mathrm{De}}}{2}\left((1-a)\sigma_{3,3}\dfrac{\partial u_1}{\partial z}-(1+a)\sigma_{1,1}\dfrac{\partial u_1}{\partial z}\right)=r\dfrac{\partial u_1}{\partial z}, \end{cases} \tag{27}$$

For the case $a=1$ (see [18]), which immediatly implies that $\sigma_{1,1}=0$, it is possible to give a simple analytic solution of this system (see [19]) and in turn a 1D Reynolds equation. This is not so easy in the present situation, as the material slip parameter a lies between -1 and 1. As a solution of Eqs. (27) is known for $\mathrm{K}=0$ (see Section 3), it is however possible to get an approximate solution for small values of K by linearization. Let us write

$$\sigma_{i,j}=\sigma_{i,j}\Big|_{\mathrm{K}=0}+\mathrm{K}\frac{\partial\sigma_{i,j}}{\partial\mathrm{K}}\Big|_{\mathrm{K}=0}+\mathcal{O}(\mathrm{K}^2).$$

Differentiating the three equations in Eqs. (27) with respect to K, we obtain

$$\begin{pmatrix} 1 & \widetilde{\mathrm{De}}(1-a)\dot\alpha & 0 \\ 0 & -\widetilde{\mathrm{De}}(1+a)\dot\alpha & 1 \\ -\widetilde{\mathrm{De}}\frac{1+a}{2}\dot\alpha & 1 & \widetilde{\mathrm{De}}\frac{1-a}{2}\dot\alpha \end{pmatrix}\begin{pmatrix} \dfrac{\partial\sigma_{1,1}}{\partial\mathrm{K}} \\ \dfrac{\partial\sigma_{1,3}}{\partial\mathrm{K}} \\ \dfrac{\partial\sigma_{3,3}}{\partial\mathrm{K}} \end{pmatrix}\Bigg|_{\mathrm{K}=0} = \begin{pmatrix} -\widetilde{\mathrm{De}}\,\sigma_{1,1}(\sigma_{1,1}+\sigma_{3,3}) \\ -\widetilde{\mathrm{De}}\,\sigma_{3,3}(\sigma_{1,1}+\sigma_{3,3}) \\ -\widetilde{\mathrm{De}}\,\sigma_{1,3}(\sigma_{1,1}+\sigma_{3,3}) \end{pmatrix}\Bigg|_{\mathrm{K}=0}$$

in which whe have defined

$$\dot\alpha=\frac{\partial u_1}{\partial z}\Big|_{\mathrm{K}=0}. \tag{28}$$

The right hand side of this system is known from Eq. (21) as it has to be computed for $\mathrm{K}=0$. Solving this system, we obtain

$$\frac{\partial\sigma_{1,3}}{\partial\mathrm{K}}\Big|_{\mathrm{K}=0}=\frac{2r^2\dot\alpha^3\widetilde{\mathrm{De}}^2a(\widetilde{\mathrm{De}}^2(1-a^2)\dot\alpha^2-1)}{(1+\widetilde{\mathrm{De}}^2(1-a^2)\dot\alpha^2)^3}, \tag{29}$$

and deduce the following approximation for small K:

$$\sigma_{1,3}\approx\left(\frac{r}{1+\widetilde{\mathrm{De}}^2(1-a^2)\dot\alpha^2}+\mathrm{K}\frac{2r^2\dot\alpha^2\widetilde{\mathrm{De}}^2a(\widetilde{\mathrm{De}}^2(1-a^2)\dot\alpha^2-1)}{(1+\widetilde{\mathrm{De}}^2(1-a^2)\dot\alpha^2)^3}\right)\dot\alpha. \tag{30}$$

When dealing with a full 3D flow, computations lead to a straightforward adaptation and the shear stress rate reads:

$$\sigma_{i,3}\approx\left(\frac{r}{1+\widetilde{\mathrm{De}}^2(1-a^2)\dot\beta^2}+\mathrm{K}\frac{2r^2\dot\beta^2\widetilde{\mathrm{De}}^2a(\widetilde{\mathrm{De}}^2(1-a^2)\dot\beta^2-1)}{(1+\widetilde{\mathrm{De}}^2(1-a^2)\dot\beta^2)^3}\right)\frac{\partial u_i}{\partial z},$$

with

$$\dot\beta^2=\left(\frac{\partial u_1}{\partial z}\right)^2+\left(\frac{\partial u_2}{\partial z}\right)^2. \tag{31}$$

Consequently, the first equation of Eqs. (25) also reads

$$\frac{\partial}{\partial z}\left(\eta_{\text{eff}}^{R}\frac{\partial \mathbf{u}}{\partial z}\right)=\nabla_{\mathbf{x}}p,$$

where

$$\eta_{\text{eff}}^{R}(\mathbf{x},z)=1-r+\frac{r}{1+\widetilde{\text{De}}^{2}(1-a^{2})\left\|\dfrac{\partial \mathbf{u}}{\partial z}(\mathbf{x},z)\right\|^{2}}+\text{K}\frac{2r^{2}\widetilde{\text{De}}^{2}\,a\left\|\dfrac{\partial \mathbf{u}}{\partial z}(\mathbf{x},z)\right\|^{2}\left(\widetilde{\text{De}}^{2}(1-a^{2})\left\|\dfrac{\partial \mathbf{u}}{\partial z}(\mathbf{x},z)\right\|^{2}-1\right)}{\left(1+\widetilde{\text{De}}^{2}(1-a^{2})\left\|\dfrac{\partial \mathbf{u}}{\partial z}(\mathbf{x},z)\right\|^{2}\right)^{3}}.$$

This expression is valid as long as K is small. However, as the magnitude of K is not known, this study aims at giving some qualitative results about the influence of the elongation number rather than quantitative results.

Relative effective viscosity $\dot{\gamma}\mapsto\eta_{\text{eff}}^{R}(\dot{\gamma})$ is plotted versus $\log(\dot{\gamma})$ for three different values of K, see Fig. 2. For $\text{K}=0$, we get the classical Rabinowisch law. For $\text{K}\leq 0.4$, the overall shape of the curve does not change, the slope decreasing as K increases. For small values of $\dot{\gamma}$, the viscosity is smaller than the one defined in the classical Rabinowisch law while it becomes greater for large values of $\dot{\gamma}$. For $\text{K}>0.4$, the overall shape becomes completely different, as the shear thinning effect tends to disappear. It is reasonable to think that the perturbation method is no longer valid. It is worth also mentioning that taking into account the elongation number in the effective viscosity law increases the range of the values of r for which the graph of the function $\dot{\gamma}\mapsto\dot{\gamma}\eta_{\text{eff}}^{R}(\dot{\gamma})$ is monotone. Then Eqs. (25)–(32) taking into account an additional elongation number may have a unique solution even for r greater than $8/9$ (see Section 5.2).

Note that in terms of real physical values, the effective viscosity reads

$$\eta_{\text{eff}}(\dot{\gamma})=\eta_{\text{visc.}}+\frac{\eta_{\text{el.}}}{1+\lambda^{2}(1-a^{2})|\dot{\gamma}|^{2}}+\frac{2\kappa\eta_{\text{el.}}\,\lambda^{2}\,a\,|\dot{\gamma}|^{2}(\lambda^{2}(1-a^{2})|\dot{\gamma}|^{2}-1)}{(1+\lambda^{2}(1-a^{2})|\dot{\gamma}|^{2})^{3}}. \tag{32}$$

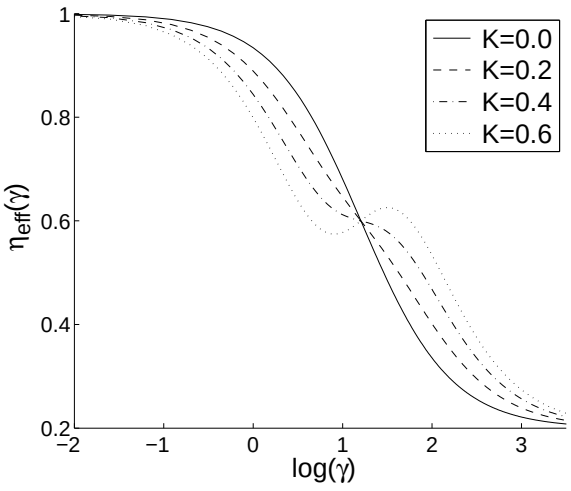

Fig. 2. Influence of the elongation correction on the relative effective viscosity as a function of the shear rate ($a=0.8$, $\widetilde{\text{De}}=0.5$, $r=0.8$)

5 Numerical simulations

In the whole section, we present numerical results that have been performed with data from Tab. 1. Although widely discussed [27, 28], homogeneous pressure boundary conditions along the boundary of the contact area have been retained for all numerical experiments with the exception of Test (G) (see Appendix B) for which an input flux is associated to the supply groove of the device.

5.1 Nonlinear Oldroyd asymptotic model: a numerical simulation

Fig. 3–4 have been performed with the data referred as Test (A) (see Tab. 1) with retardation parameter $r = 0.8$ and Deborah number $\widetilde{\mathrm{De}} = 1.3$ (notice that 3D profiles are presented in the unit cube where the third direction, which is orthogonal to the shear plan, has been rescaled as $Z := z/h(\mathbf{x})$). In particular,

- Fig. 3 (left) represents the pressure distribution in the thin film. More details will be given later on the effects of the Oldroyd contribution on the pressure distribution.
- Fig. 3 (right) represents the distribution of the effective rescaled viscosity defined by

$$\eta_{\mathrm{eff}}^{R}(\mathbf{x},z) := 1 - r + \frac{r}{1 + (1-a^2)\widetilde{\mathrm{De}}^2 \left\| \dfrac{\partial \mathbf{u}}{\partial z}(\mathbf{x},z) \right\|^2}. \tag{33}$$

  In the Newtonian case, the effective relative viscosity is uniformly equal to 1 ; in the Oldroyd model, velocity gradients lead to a non-uniform distribution of the effective viscosity, which varies from $1-r$ to 1.
- Fig. 4 represents the distribution of the stress tensor components. More details will be given later on the effects of the Oldroyd contribution concerning these variables.

5.2 Influence of the elongation correction

As previously mentioned, the range of validity for the retardation parameter r is wider using the elongation correction. Numerical simulation referred as Test (B) (see Tab. 1) presents the following results. Pressure profiles are plotted on Fig. 5 for various parameters around the upper limit $r = 8/9$ with $a = 0.2$ and $\widetilde{\mathrm{De}} = 0.72$. Let us recall that, for $\mathrm{K} = 0$, the algorithm cannot capture the solution as $r > 8/9$ (as the problem is ill-posed). Fortunately, for $r = 0.91$, the choice $\mathrm{K} = 0.82$ allows us to get a solution (the problem becomes well-posed thanks to the PTT correction), which can be compared to the solution of the problem with values such as $(r,\mathrm{K}) = (0.88, 0.79)$ and $(r,\mathrm{K}) = (0.88, 0.00)$. Thus Fig. 5 presents the results related to the pressure distribution, at least when the problem is well-posed.

Fig. 6–7 presents the results related to the stress components at the shearing surface by focusing on the influence on the elongation number: the value of K is moderate but leads to significant change in the shape of the stress profiles.

5.3 About the perturbation method with respect to the Deborah number

As mentionned in the first section, a perturbation-asymptotic approach has been proposed by J. Tichy [18] for the upper convective Maxwell (UCM) model ($a = 1$, $r = 1$). Assuming a linear dependence with respect to the Deborah parameter, it is assumed that the (real) viscoelastic pressure p_{De} is related to the Newtonian one p_0 by the following relationship

$$p_{\mathrm{De}} = p_0 + \mathrm{De}\, p^{(c)}, \tag{34}$$

where $p^{(c)}$ is a corrective pressure. As soon as $p^{(c)}$ is computed, it is possible to know the real pressure for any small De by an elementary additive procedure. In the present situation corresponding to the case $-1 < a < 1$ and $0 < r < 1$, it is noteworthy that the previous expansion is not relevant (see Tab. 2, obtained with the numerical parameters presented as Test (C), see Tab. 1). By selecting different values of r, introducing the load

$$L := \iint_{\omega} p(\mathbf{x})\, \mathrm{d}\mathbf{x}, \tag{35}$$

we prove numerically that, for all values of the retardation parameter which are less than 8/9, the difference of pressure mean values between the non-Newtonian case and the Newtonian case behaves as $o(\widetilde{\mathrm{De}}^2)$ for small values of $\widetilde{\mathrm{De}}$ (see, for instance, Fig. 8), i. e.

$$p_{\widetilde{\mathrm{De}}} = p_0 + \widetilde{\mathrm{De}}^2\, p^{(c)}. \tag{36}$$

	(A)	**(B)**
	Fig. 3-4, 9-10	Fig. 5-6-7
Fluid domain:		
Domain ω	$[0,1]\times[0,1]$	$[0,1]\times[0,1]$
Gap $h(\mathbf{x})$	$1-0.8x_1$	$1-0.8x_1$
Shear velocity $\mathbf{s}$	$(1,0)$	$(1,0)$
Rheological data:		
Retardation parameter r	$0.00\sim0.80$	$0.88\sim0.91$
Deborah number $\widetilde{\mathrm{De}}$	1.30	0.72
Material slip parameter a	0.80	0.80
Elongation number K	0.00	$0.00\sim0.82$
Boundary conditions:	$p=0$	$p=0$
Numerical parameters:		
Mesh numbers	$40\times20\times20$	$40\times20\times20$
Artificial time step δ	10^{-3}	10^{-4}
Equilibrium parameter r_p/δ	10^{-4}	10^{-4}

	(C)	**(D)**
	Fig. 8, Tab. 2	Tab. 3
Fluid domain:		
Domain ω	$[0,1]\times[0,5]$	$[0,1]\times[0,1]$
Gap $h(\mathbf{x})$	$1+H'x_1+0.5H''(x_1^2-x_1)$	$1-0.25x_1$
Shear velocity $\mathbf{s}$	$(1,0)$	$(1,0)$
Rheological data:		
Retardation parameter r	$0.75\sim0.85$	$0.00\sim0.80$
Deborah number $\widetilde{\mathrm{De}}$	$0.00\sim2.50$	$0.00\sim1.80$
Material slip parameter a	0.80	0.80
Elongation number K	0.00	$0.00\sim0.16$
Boundary conditions:	$p=0$	$p=0$
Numerical parameters:		
Mesh numbers	$40\times20\times40$	$40\times40\times10$
Artificial time step δ	10^{-3}	10^{-4}
Equilibrium parameter r_p/δ	10^{-4}	10^{-3}

Table 1. Numerical data (numerical parameters are related to the algorithm, see Appendix C)

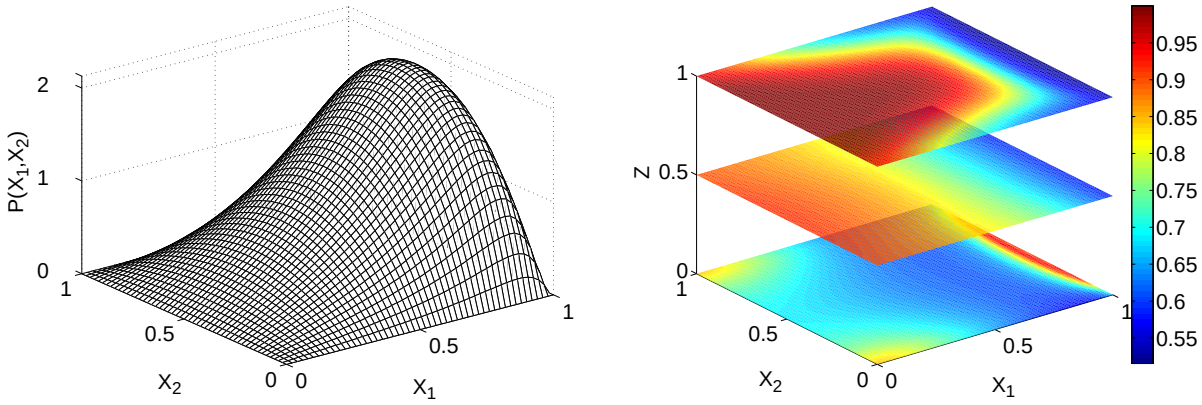

Fig. 3. Pressure distribution (left) and effective viscosity including Oldroyd contribution: $(x_1,x_2,z) \mapsto \eta_{\text{eff}}^R(x_1,x_2,z)$ (right) in the linear converging profile with $r = 0.8$, $\widetilde{\text{De}} = 1.3$ and $a = 0.8$

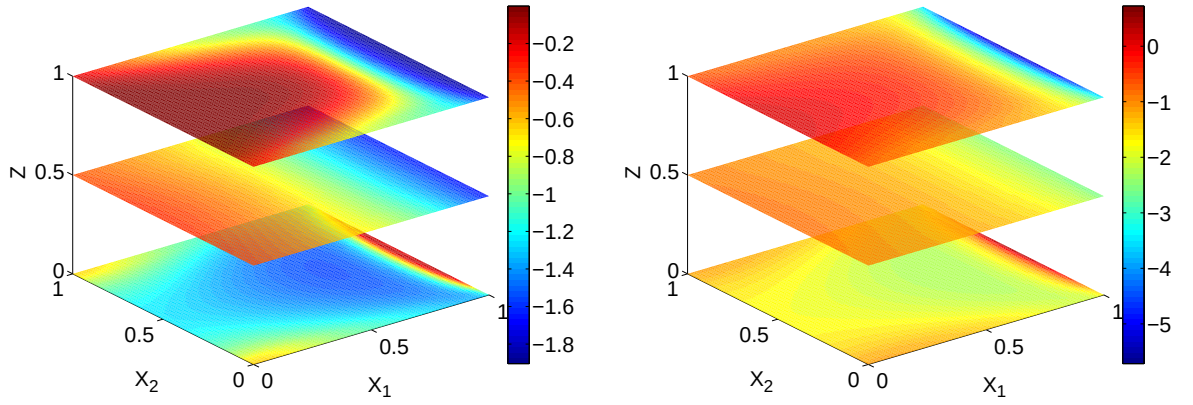

Fig. 4. Stress $(x_1,x_2,z) \mapsto (\sigma_{11} - \sigma_{33})(x_1,x_2,z)$ (left) and $(x_1,x_2,z) \mapsto \sigma_{13}(x_1,x_2,z)$ (right) in the linear converging profile with $r = 0.8$, $\widetilde{\text{De}} = 1.3$ and $a = 0.8$

Moreover, when the Deborah number is not too small, the quadratic behaviour of the pressure is not valid anymore, as shown on Fig. 8. In this work, we emphasize that our model does not rely on any assumption on the amplitude of the Deborah number and a numerical solution can be computed without smallness restriction on $\widetilde{\text{De}}$, unlike J. Tichy's work. Notice that our results have been obtained with the same data as J. Tichy's, adapted to the 2D case (J. Tichy's results are 1D), i. e. in a domain $(0,1) \times (0,5)$.

	$r = 0.25$	$r = 0.50$	$r = 0.75$	$r = 0.80$	$r = 0.85$
$H' = -0.8, H'' = -1$	1.941	1.893	1.928	1.947	1.978
$H' = -0.8, H'' = +1$	2.128	1.990	1.985	1.994	2.008

Table 2. Order of convergence of the load with respect to the Deborah number, for small values of $\widetilde{\text{De}}$

5.4 Influence of the parameters on the load

Numerical simulations, here referred as Test (D) (see Tab. 1), investigate the influence of the retardation parameter r, the Deborah number $\widetilde{\text{De}}$ and the elongation number K over the load. For any value of the retardation parameter r, numerical results highlight some general trend (see Tab. 3: for moderate values of $\widetilde{\text{De}}$, then the load computed with the perturbation

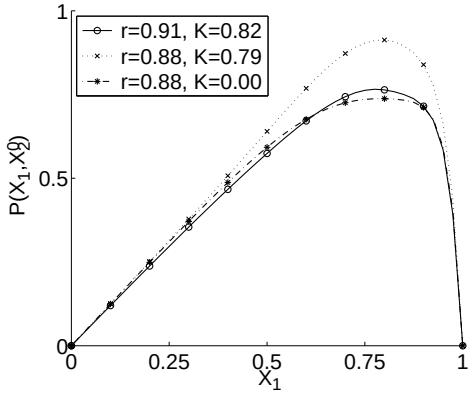

Fig. 5. Pressure distribution $x_1 \mapsto p(x_1, x_2^0)$, following the streamline $x_2^0 := D/2$, in the (linear) converging profile. Influence of the elongation number (other parameters are: $a = 0.80$, $\widetilde{\mathrm{De}} = 0.72$

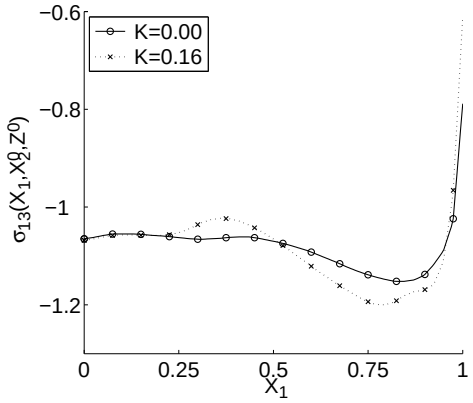

Fig. 6. Stress component $x_1 \mapsto (\sigma_{13})(x_1, x_2^0, z^0)$, following the streamline $x_2^0 := D/2$ at the shearing surface $z^0 := 0$, in the (linear) converging profile. Influence of the elongation number (other parameters are: $r = 0.88$, $a = 0.80$, $\widetilde{\mathrm{De}} = 0.72$)

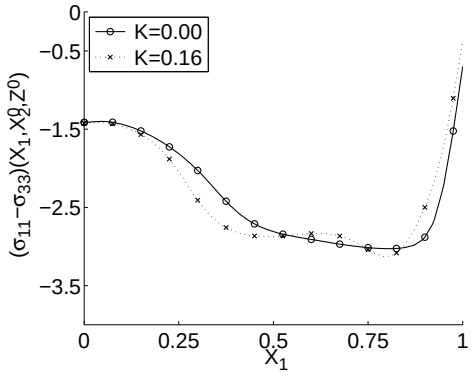

Fig. 7. Stress component $x_1 \mapsto (\sigma_{11} - \sigma_{33})(x_1, x_2^0, z^0)$, following the streamline $x_2^0 := D/2$ at the shearing surface $z^0 := 0$, in the (linear) converging profile. Influence of the elongation number (other parameters are: $r = 0.88$, $a = 0.80$, $\widetilde{\mathrm{De}} = 0.72$)

corrector (i. e. $\mathrm{K} = 0.2 \cdot r$ in our simulation) is less than the load computed with $\mathrm{K} = 0.0$; then, when $\widetilde{\mathrm{De}}$ becomes greater than 1, the load computed with the perturbation corrector is greater than the load computed with $\mathrm{K} = 0.0$.

6 Conclusion

Upper convective model (UCM) assumption is often retained for studying viscoelastic thin film flows. Deleting this assumption, it has been possible to prove that for a convenient choice of governing parameters, thin film flows based upon an Phan-Thien Tanner / Oldroyd-B viscoelastic model can be completely described by a double Newtonian (modified) Ra-

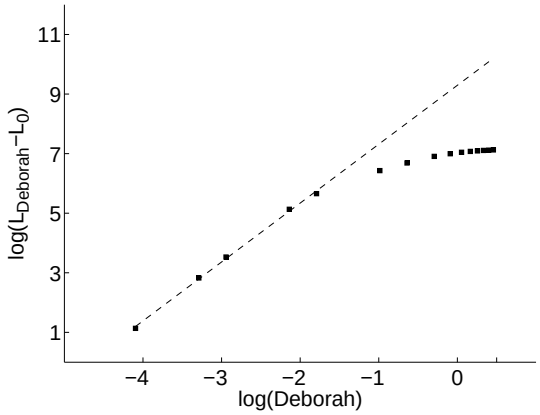

Fig. 8. Convergence of the load difference $L_{\widetilde{\mathrm{De}}} - L_0$ with respect to the Deborah number, with a retardation parameter $r = 0.85$ and in the geometry $H' = -0.8$, $H'' = -1$, and with $a = 0.8$. For small values of $\widetilde{\mathrm{De}}$, the slope of the graph is approximatively equal to 2

Load$*$1e+3	$r = 0.2$	$r = 0.5$	$r = 0.8$
$\widetilde{\mathrm{De}} = 0.0$	75.45 ($\pm$00.00)	75.45 ($\pm$00.00)	75.45 ($\pm$00.00)
$\widetilde{\mathrm{De}} = 0.2$	75.21 ($-$00.23)	74.84 ($-$00.80)	74.35 ($-$01.93)
$\widetilde{\mathrm{De}} = 0.5$	73.64 ($-$01.62)	68.66 ($-$04.18)	63.44 ($-$06.91)
$\widetilde{\mathrm{De}} = 0.8$	70.32 ($-$01.00)	59.92 ($-$02.38)	48.39 ($-$03.46)
$\widetilde{\mathrm{De}} = 1.2$	66.67 ($+$01.12)	50.25 ($+$03.47)	30.69 ($+$07.98)
$\widetilde{\mathrm{De}} = 1.5$	64.86 ($+$02.13)	45.57 ($+$06.12)	22.03 ($+$13.10)
$\widetilde{\mathrm{De}} = 1.8$	63.67 ($+$02.46)	42.64 ($+$06.84)	16.98 ($+$14.14)

Table 3. Load in the viscoelastic case for various values of r and $\widetilde{\mathrm{De}}$. For each set of parameters, the entry corresponds to the load without elongation correction i. e. $\mathrm{K} = 0.0$ (resp. load *deviation* due to the elongation correction $\mathrm{K} = 0.2 \cdot r$)

binowisch effective viscosity law. Using a new algorithm, influence of the various parameters has been described for the pressure and for the stress tensor. The detailed distribution of the viscosity in the contact area has been presented and shows that shear thinning effect takes place even for very moderate operating conditions. Further non linear effects due to the elongation numbers can be taken into account by way of a perturbation method, so leading to a modified Rabinowisch law. As a consequence, a reduction in the load capacity is obtained for small Deborah numbers while a load increase is gained for greater Deborah numbers.

Acknowledgments : Authors are grateful for various discussions with B. Bou-Said and P. Vergne, from INSA Lyon.

References

[1] Boucherit, H., Lahmar, M., Bou-Said, B., and Tichy, J., 2010. "Comparison of non-Newtonian constitutive laws in hydrodynamic lubrication". *Tribology Letters*, **40**(1), pp. 49–57.

[2] Carreau, D. J., Kee, D. D., and Daroux, M., 1979. "An analysis of the viscous behaviour of polymeric solutions". *The Canadian Journal of Chemical Engineering*, **57**(2), pp. 135–141.

[3] Yasuda, K., Armstrong, R. C., and Cohen, R. E., 1981. "Shear flow properties of concentrated solutions of linear and star branched polystyrenes". *Rheologica Acta*, **20**(2), pp. 163–170.

[4] Bair, S., and Khonsari, M. M., 2005. "Generalized Reynolds equations for line contact with double-Newtonian shear-thinning". *Tribology Letters*, **18**(4), pp. 513–520.

[5] Bair, S., and Qureshi, F., 2003. "The high pressure rheology of polymer-oil solutions". *Tribology International*, **36**(8), pp. 637–645.

[6] Bair, S., 2002. "The shear rheology of thin compressed liquid films". *Proceedings of the Institution of Mechanical Engineers, Part J: Journal of Engineering Tribology*, **216**(1), pp. 1–17.
[7] Bair, S., and Qureshi, F., 2003. "The generalized Newtonian fluid model and elastohydrodynamic film thickness". *ASME Journal of Tribology*, **125**(1), pp. 70–75.
[8] Bair, S., Vergne, P., and Marchetti, M., 2002. "The effect of shear-thinning on film thickness for space lubricants". *STLE Tribology Transactions*, **45**(3), pp. 330–333.
[9] Cross, M. M., 1965. "Rheology of non-Newtonian fluids: A new plot for pseudoplastic systems". *Journal of Colloid Science*, **20**(5), pp. 417–437.
[10] Bair, S., 2006. "A Reynold-Ellis equation for line contact with shear-thinning". *Tribology International*, **39**(4), pp. 310–316.
[11] Bair, S., and Khonsari, M. M., 2006. "Reynolds equation for common generalized Newtonian models and an approximate Reynolds-Carreau equation". *Proceedings of the Institution of Mechanical Engineers, Part J: Journal of Engineering Tribology*, **220**(4), pp. 365–374.
[12] Lin, J. R., 2001. "Non-Newtonian effects on the dynamic characteristics of one-dimensional slider bearings: Rabinowisch fluid model". *Tribology Letters*, **10**(4), pp. 237–243.
[13] Swamy, S. T. N., Prabhu, B. S., and Rao, B. V. A., 1975. "Stiffness and damping characteristics of finite width journal bearings with a non-Newtonian film and their application to instability prediction". *Wear*, **32**(3), pp. 379–390.
[14] Conry, T. F., Wang, S., and Cusano, C., 1987. "A Reynolds Eyring equation for elastohydrodynamic lubrication in line contacts". *ASME Journal of Tribology*, **109**(4), pp. 648–658.
[15] Ehret, P., Dowson, D., and Taylor, C. M., 1998. "On lubricant transport conditions in elasto-hydrodynamic conjunctions". *Proceedings of the Royal Society A*, **454**(1971), pp. 763–787.
[16] Hooke, C. J., 2000. "The behaviour of low-amplitude surface roughness under lines contacts: non-Newtonian fluids". *Proceedings of the Institution of Mechanical Engineers, Part J: Journal of Engineering Tribology*, **214**(3), pp. 253–265.
[17] Greenwood, J. A., 2000. "Two-dimensional flow of a non-Newtonian lubricant". *Proceedings of the Institution of Mechanical Engineers, Part J: Journal of Engineering Tribology*, **214**(1), pp. 29–41.
[18] Tichy, J., 1996. "Non-Newtonian lubrication with the convective Maxwell model". *ASME Journal of Tribology*, **118**(2), pp. 344–349.
[19] Talay Akyildiz, F., and Bellout, H., 2004. "Viscoelastic lubrification with Phan-Thien-Tanner fluid (PTT)". *ASME Journal of Tribology*, **126**(2), pp. 288–291.
[20] Zhang, R., and Li, X. K., 2005. "Non-Newtonian effects on lubricant thin film flows". *Journal of Engineering Mathematics*, **51**(1), pp. 1–13.
[21] Georgiou, G. C., and Vlassopoulos, D., 1998. "On the stability of the simple shear flow of a Johnson-Segalman fluid". *Journal of Non-Newtonian Fluid Mechanics*, **75**(1), pp. 77–97.
[22] Fyrillas, M. M., Georgiou, G. C., and Vlassopoulos, D., 1999. "Time dependant plane Poiseuille flow of a Johnson-Segalman fluid". *Journal of Non-Newtonian Fluid Mechanics*, **82**(1), pp. 105–123.
[23] Bayada, G., Chupin, L., and Grec, B., 2009. "Viscoelastic fluids in thin domains: a mathematical proof". *Asymptotic Analysis*, **64**(3-4), pp. 185–211.
[24] Tanner, R. I., and Walters, K., 1998. *Rheology: an historical perspective*, Vol. 7 of *Rheology series*. Elsevier, Amsterdam. 268 pp.
[25] Joseph, D. D., 1998. *Fluid dynamics of viscoelastic liquids*, Vol. 84 of *Applied Mathematical Sciences*. Springer, New York. 754 pp.
[26] Bayada, G., Chupin, L., and Martin, S., 2007. "Viscoelastic fluids in a thin domain". *Quarterly of Applied Mathematics*, **65**(4), pp. 625–651.
[27] Szeri, A. Z., 1998. *Fluid film lubrication: theory and design*. Cambridge University Press, New York. 428 pp.
[28] Tanner, R. I., 2000. *Engineering rheology*, Vol. 52 of *Oxford Engineering Science Series*. Oxford University Press, New York. 592 pp.

In the appendix, we present some complementary results, with data presented on Tab. 4.

A Influence of rheological parameters in the asymptotic model

A.1 Influence of the retardation parameter

Fig. 9–10 focus on the influence of the retardation parameter on the solution. The Deborah number is taken as $\widetilde{\mathrm{De}} = 1.3$. Other data are presented in Tab. 1 (see Test (A)). Starting from the pressure of the Newtonian problem with viscosity 1 ($r = 0$), we can observe that the solution highly depends on r (computations cannot be performed for values greater than $8/9$ due to ill-posedness of the problem and, consequently, non-convergence of the algorithm). The pressure tends to decrease as the retardation parameter increases ; elastic effects also modify in a significant way the shear stress located at the shearing surface, thus suggesting that the rheological properties (such as the retardation parameter) are among the major determinants

	(E)	**(F)**
	Fig. 11-14	Fig. 15, Tab. 5
Fluid domain:		
Domain ω	$[0,1]\times[0,1]$	$[0,1]\times[0,1]$
Gap $h(\mathbf{x})$	$1-0.8\,x_1$	$1-(1-H_{\min})\,x_1$
Shear velocity $\mathbf{s}$	$(1,0)$	$(1,0)$
Rheological data:		
Retardation parameter r	0.80	0.70 | 0.30
Deborah number $\widetilde{\mathrm{De}}$	$0.00\sim\infty$	0.72
Material slip parameter a	0.80	0.80
Elongation number K	0.00	0.00
Boundary conditions:	$p=0$	$p=0$
Numerical parameters:		
Mesh numbers	$40\times20\times20$	$80\times20\times40$
Artificial time step δ	10^{-3}	10^{-4}
Equilibrium parameter r_p/δ	10^{-4}	10^{-4}

	(G)
	Fig. 16
Fluid domain:	
Domain ω	$[0,1]\times[0,5]$
Gap $h(\mathbf{x})$	$(2x_1-1)^2+0.5$
Shear velocity $\mathbf{s}$	$(1,0)$
Rheological data:	
Retardation parameter r	$0.00\sim0.70$
Deborah number $\widetilde{\mathrm{De}}$	1.30
Material slip parameter a	0.80
Elongation number K	0.00
Boundary conditions:	
Conditions at $x_1=0$	flux
Conditions on other boundaries	$p=0$
Numerical parameters:	
Mesh numbers	$40\times80\times20$
Artificial time step δ	10^{-4}
Equilibrium parameter r_p/δ	10^{-4}

Table 4. Numerical data

of the lubricants efficiency.

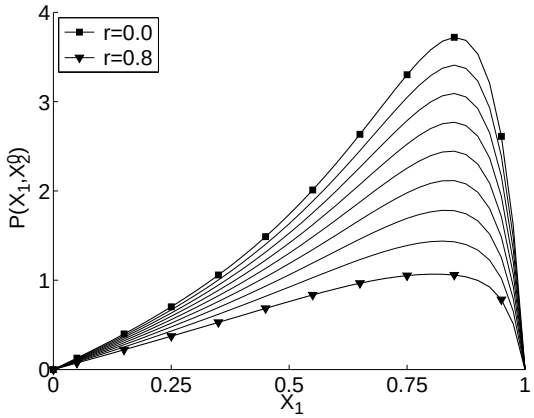

Fig. 9. Pressure distribution $x_1 \longrightarrow p(x_1, x_2^0)$, following the streamline $x_2^0 := D/2$, in the (linear) converging profile with $\widetilde{\mathrm{De}} = 1.3$ and for different values of the retardation parameter $r = 0.1, 0.2, ..., 0.8$

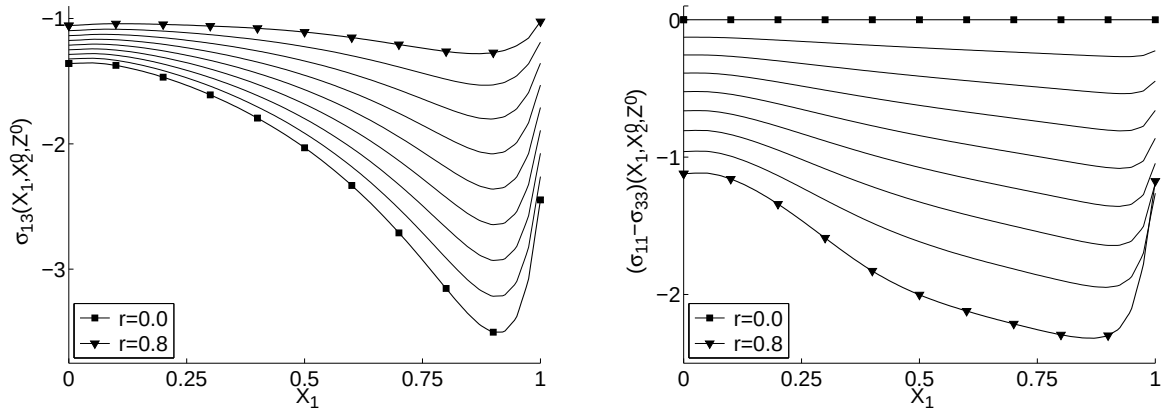

Fig. 10. Component of the constraint tensor $x_1 \longrightarrow \sigma_{13}(x_1, x_2^0, z^0)$ (left), $x_1 \longrightarrow (\sigma_{11} - \sigma_{33})(x_1, x_2^0, z^0)$ (on right) following the streamline $x_2^0 := D/2$ at the shearing surface $z^0 := 0$, in the (linear) converging profile with $\widetilde{\mathrm{De}} = 1.3$ and for different values of the retardation parameter $r = 0.1, 0.2, ..., 0.8$

A.2 Influence of the Deborah number and material slip parameter

Let us remark that, in Eq. (26), the Deborah number $\widetilde{\mathrm{De}}$ and the material slip parameter a can be reduced into one single parameter, as the effective viscosity law only depends on the parameter $\widetilde{\mathrm{De}}^2(1-a^2)$ (of course, this does not hold anymore when taking into account the influence of the elongation number, i. e. $\mathrm{K} \neq 0$). Therefore, we choose to impose $a = 0.8$ and let De vary from 0 to large values. In that prospect, Fig. 11–14 focus on the influence of the Deborah number. The numerical experiment is referred as Test (E) (see Tab. 4). The retardation parameter is taken as $r = 0.8$. Starting from the pressure of the Newtonian problem with viscosity 1 ($\widetilde{\mathrm{De}} = 0$), we can observe that increasing the value of $\widetilde{\mathrm{De}}$ tends to decrease the pressure, until converging to a pressure which is identified to the solution of the Newtonian problem with viscosity $1-r$. In a similar way, we would observe that the behaviour of the shear stress σ_{13} obeys the same trend (therefore, the corresponding figure is volunteerily omitted): increasing the value of the Deborah number leads (in a monotone way) the initial solution (Newtonian solution with effective viscosity uniformly equal to 1) to a limit solution identified as a Newtonian solution with effective viscosity $1-r$, the path being nonlinear due to elastic effects. However, dependency with respect to the Deborah number may not be monotone, as for $\sigma_{11} - \sigma_{33}$, see Fig. 12-14. In both Newtonian regimes ($\widetilde{\mathrm{De}} = 0$ and $\widetilde{\mathrm{De}} = +\infty$), the computation of the solution leads to $\sigma_{11} - \sigma_{33} = 0$ at $x_2^0 = D/2$, $z^0 = 0$, but the path between those two regimes is the following one:

– Fig. 12 shows that, in the chosen configuration, $\sigma_{11} - \sigma_{33}(\cdot, x_2^0, z^0)$ decreases with respect to $\widetilde{\mathrm{De}}$ for small values of $\widetilde{\mathrm{De}}$

only ;

– Fig. 13 reveals the change of the trend: monotonicity fails at intermediate values of $\widetilde{\mathrm{De}}$;
– Fig. 14 shows that, in the chosen configuration, $\sigma_{11} - \sigma_{33}(\cdot, x_2^0, z^0)$ increases with respect to $\widetilde{\mathrm{De}}$ for large values of $\widetilde{\mathrm{De}}$.

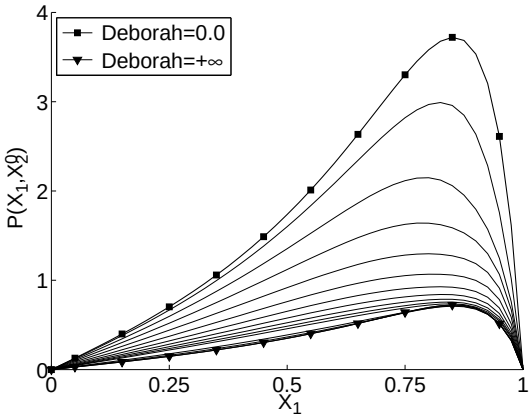

Fig. 11. Pressure distribution $x_1 \mapsto p(x_1, x_2^0)$, following the streamline $x_2^0 := D/2$, in the (linear) converging profile with $r = 0.8$ and for different values of the Deborah number $\widetilde{\mathrm{De}} = 0.1, 0.2, ..., 5.0$

A.3 Effective viscosity in the Oldroyd-B thin film flow

In this subsection, we study the influence of the Oldroyd-B model on the effective viscosity. Numerical parameters are presented in Tab. 4, referred as Test (F). In this non-Newtonian regime, we have focused on a flow which is compressed in a linear profile, the maximal gap being fixed to 1, the minimal gap $H_{\min}$ varying from 0.90 to 0.01.

From the equations, we infer that the effective viscosity varies from $1 - r$ and 1. Fig. 15 illustrates the distribution of the three-dimensional effective viscosity within the theoretical range, for different values of $H_{\min}$. It is observed that decreasing values of $H_{\min}$ tend to spread the distribution. More precisely, high velocity gradients, here associated to minimal gap thickness, lead to reach the minimal effective viscosity: large values of $H_{\min}$ are not sufficient to cover the whole range of values, although small values of $H_{\min}$ widen the range of values and tend to spread the distribution from the minimal value to the maximal one. This is mainly due to the fact that small values of $H_{\min}$ lead to high velocity gradients, thus diminishing the effective velocity. This is also represented by Tab. 5 which provides the mean value of the effective viscosity in the 3D domain, the standard deviation with respect to this mean value and the numerical range which is reached.

$H_{\min}$	mean value	standard deviation	min. value	max. value
0.90	0.848	0.010	0.806	0.884
0.50	0.775	0.078	0.434	0.970
0.20	0.689	0.170	0.314	1.000
0.10	0.664	0.214	0.304	1.000
0.05	0.658	0.233	0.301	1.000
0.01	0.643	0.243	0.300	1.000

Table 5. Heterogeneity of the effective viscosity distribution in the viscoelastic fluid flow ($r = 0.7$, $\mathrm{De} = 0.72$, $a = 0.8$), depending on the converging profile

Fig. 15 represents the same computation, adapted to the two-dimensional average effective viscosity, defined as

$$\overline{\eta^R_{\rm eff}}(\mathbf{x}) := \frac{1}{h(\mathbf{x})}\int_0^{h(\mathbf{x})} \eta^R_{\rm eff}(\mathbf{x},z)\,{\rm d}z. \tag{37}$$

in order to give some comprehensive details on the effective viscosity associated to the thin film flow. Although the effective viscosity distribution significantly reaches values greater than 0.9, the average effective viscosity never reaches such values. This means that the effective viscosity is not homogeneous in the thin film thickness direction. It also means that variations of velocity gradients (associated to the measure of the effective viscosity) may be important in the thin film thickness, at least for small values of the gradients. As a consequence, this reveals the heterogeneous properties of the viscoelastic fluid flow with respect to the direction orthogonal to the shearing surface (i. e. in the thin film thickness).

B Boundary effects due to elastic perturbation

Fig. 16 represents the pressure distribution for different values of the retardation parameter. The geometry relies on a converging-diverging profile (see Tab. 4, Test (G)) with an imposed flux $\mathbf{q} = 0.2\,\mathbf{s}h(0,\cdot)$ at $x_1 = 0$. The dimensions of the domain fall into the scope of the journal bearing of infinite width assumption, as $0 < x_1^\star < 1$ and $0 < x_2^\star < 5$. In the Newtonian regime, it is observed that the infinite width approximation is valid, leading to the use of 1D reduced models instead of 3D initial systems ; in the non-Newtonian situation, the numerical result suggests that such an assumption may be not valid anymore when the retardation parameter becomes too large.

C Numerical algorithm

This method is based on a fixed point procedure. The first idea is to consider that the unknown velocity-pressure $(\mathbf{u}, p)$ (solution of Eqs. (25) and (26) or, if considering the PTT correction, Eqs. (25) and (32)) can be computed as the limit as n tends to infinity of a sequence $(\mathbf{u}_n, p_n)$ solution of

$$\frac{\partial}{\partial z}\left(F(\mathbf{u}^{n-1})\frac{\partial \mathbf{u}^n}{\partial z}\right) = \nabla p^n, \qquad \mathrm{div}\left(\int_0^H \mathbf{u}^n(\cdot,z)\,dz\right) = 0, \tag{38}$$

in which function F is related to the viscosity law, namely

$$F(\mathbf{u}) = 1 - r + \frac{r}{1 + \widetilde{\mathrm{De}}^2(1-a^2)\left\|\dfrac{\partial \mathbf{u}}{\partial z}\right\|^2},$$

without the PTT correction, or

$$F(\mathbf{u}) = 1 - r + \frac{r}{1 + \widetilde{\mathrm{De}}^2(1-a^2)\left\|\dfrac{\partial \mathbf{u}}{\partial z}\right\|^2} + \mathrm{K}\frac{2r^2\widetilde{\mathrm{De}}^2 a\left\|\dfrac{\partial \mathbf{u}}{\partial z}\right\|^2\left(\widetilde{\mathrm{De}}^2(1-a^2)\left\|\dfrac{\partial \mathbf{u}}{\partial z}\right\|^2 - 1\right)}{\left(1 + \widetilde{\mathrm{De}}^2(1-a^2)\left\|\dfrac{\partial \mathbf{u}}{\partial z}\right\|^2\right)^3},$$

with the PTT correction.

In turn, $(\mathbf{u}_n, p_n)$ are computed for each value of the index n as the limit of the solution of a fixed-point problem (introducing new index k).

$$\frac{\partial}{\partial z}\left(F(\mathbf{u}^{n-1})\frac{\partial \mathbf{u}^{n,k+1}}{\partial z}\right) = \nabla p^{n,k}, \qquad p^{n,k+1} - p^{n,k} + \delta\,\mathrm{div}\left(\int_0^H \mathbf{u}^n(\cdot,z)\,dz\right) = 0, \tag{39}$$

in which δ is an artificial penalization parameter.

In order to solve Eq. (38), a semi-discretization in the (x_1, x_2)-direction is introduced. We use a centered structured grid based on a classical cell configuration (see Fig. 17, for a rectangular domain with a size $L \times D$).

Let us denote by $N = N_1 \times N_2$ the overall number of unknowns corresponding to this discretisation, by δ_1 (resp. δ_2) the step in the x_1 (resp. x_2) direction, by h_{ij} the value of h at a node (i, j). Furthermore, we denote

$$\begin{array}{c} \mathbf{U}(z) = (\mathbf{u}_{ij}(z)) := (\mathbf{u}(i\delta_{x_1}, j\delta_{x_2}, z)) \\ P = (p_{ij}) := (p(i\delta_{x_1}, j\delta_{x_2})) \end{array} \tag{40}$$

the semi-discretized horizontal velocity and discretized pressure.

Let A (resp. B) correspond to the $\mathbf{x}$-discretisation of the operator ∇ (resp. div). We use the notation

$$\left(\widetilde{H\mathbf{U}}\right)_{ij} := \int_0^{h_{ij}} \mathbf{u}_{ij}(z)\, dz. \tag{41}$$

The overall procedure reads now:

$$\text{Loops on } n\text{:} \begin{cases} \mathbf{U}^{n,0} = \mathbf{U}^n, \quad P^{n,0} = P^n, \\ \text{Loops on } k\text{:} \begin{cases} -\dfrac{\partial}{\partial z}\left(F(\mathbf{U}^n)\dfrac{\partial \mathbf{U}^{n,k+1}}{\partial z}\right) + A \circ P^{n,k} = \mathbf{0}, \\ P^{n,k+1} - P^{n,k} + \delta B \circ \left(\widetilde{H\mathbf{U}}^{n,k+1}\right) = 0, \end{cases} \\ \mathbf{U}^{n+1} = \mathbf{U}^{n,\infty}, \quad P^{n+1} = P^{n,\infty}. \end{cases}$$

This internal problem is a linear one as the computation of the new pressure $p^{n,k+1}$ is an explicit procedure while the computation of the velocity $\mathbf{u}^{n,k+1}$ is obtained by solving a set of ordinary partial differential equations in the $z-$direction, which is equivalent to solve a linear system of equations after a discretization in the $z-$direction (N_z nodes).

The stopping test of the internal loop is based on the pressure error $P^{n,k+1} - P^{n,k}$ and on the velocity error $\mathbf{U}^{n,k+1} - \mathbf{U}^{n,k}$. Note that the precision sought in pressure will induce a precision on the incompressibility condition via the parameter δ. In fact, the algorithm is stopped as soon as $|P^{n,k+1} - P^{n,k}|$ is smaller than a prescribed value, noted r_p. If this condition is satisfied, it means in particular that the divergence term satisfies

$$\max_{ij} \left| \left(B \circ \left(\widetilde{H\mathbf{U}}^{n,k+1}\right)\right)_{ij} \right| \leq \frac{r_p}{\delta}, \tag{42}$$

i. e. the free divergence equality is satisfied with an order of r_p/δ. For this reason r_p/δ will be called the "equilibrium parameter (for the free divergence condition)". In order to numerically attain the free divergence equality, we have to impose some value for r_p satisfying $r_p \ll \delta$.

Numerical experiments show that $\delta = 10^{-3}$ and $r = 10^{-4}\delta$ ensure good convergence for $N_1 = 40$, $N_2 = 40$ and $N_z = 20$, see [26].

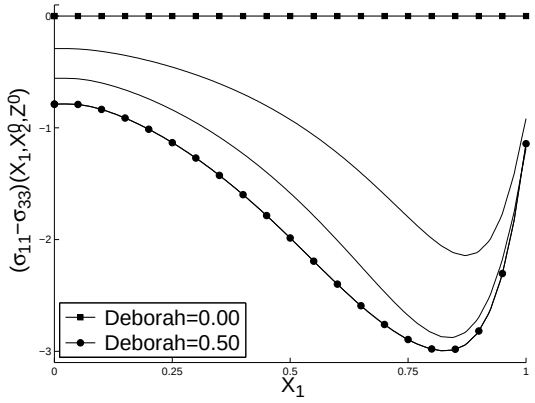

Fig. 12. Stress component $x_1 \mapsto (\sigma_{11}-\sigma_{33})(x_1,x_2^0,z^0)$, following the streamline $x_2^0 := D/2$ at the shearing surface $z^0 := 0$, in the (linear) converging profile with $r = 0.7$ and for different values of the Deborah number $\widetilde{\mathrm{De}} = 0.00, 0.17, 0.33, 0.50$

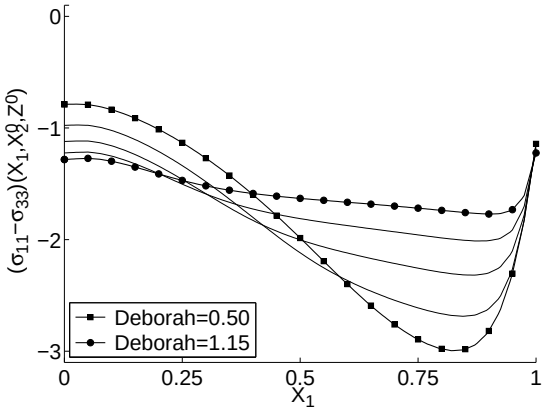

Fig. 13. Stress component $x_1 \mapsto (\sigma_{11}-\sigma_{33})(x_1,x_2^0,z^0)$, following the streamline $x_2^0 := D/2$ at the shearing surface $z^0 := 0$, in the (linear) converging profile with $r = 0.7$ and for different values of the Deborah number $\widetilde{\mathrm{De}} = 0.5, 0.65, 0.80, 0.95, 1.15$

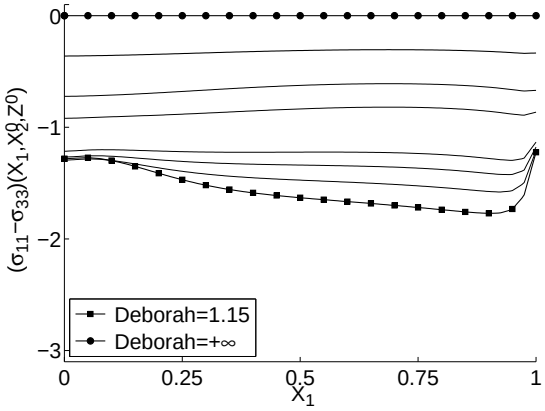

Fig. 14. Stress component $x_1 \mapsto (\sigma_{11}-\sigma_{33})(x_1,x_2^0,z^0)$, in the (linear) converging profile with $r = 0.7$ and for different values of the Deborah number $\widetilde{\mathrm{De}} = 1.15, 1..33, 1.50, 1.60, 3.33, 5.00; +\infty$

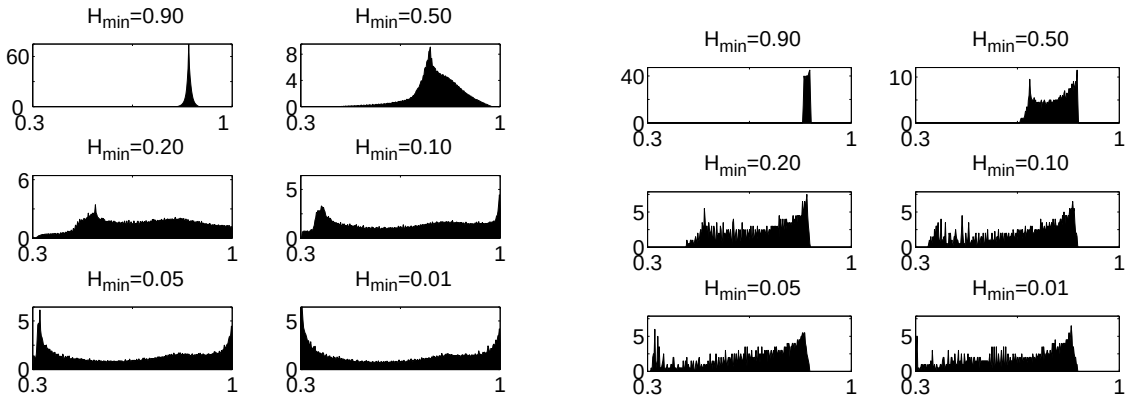

Fig. 15. **left:** Percentage distribution of the effective viscosity in the three dimensional thin film flow, for different values of $H_{\min}$, in a non-Newtonian regime ($\widetilde{\mathrm{De}} = 0.72$, $r = 0.7$ and $a = 0.8$). **right:** Percentage distribution of the *average* effective viscosity *in the two dimensional thin film flow*, for different values of $H_{\min}$, in a non-Newtonian regime ($\widetilde{\mathrm{De}} = 0.72$, $r = 0.7$ and $a = 0.8$). Effective viscosity varies from $1 - r$ to 1

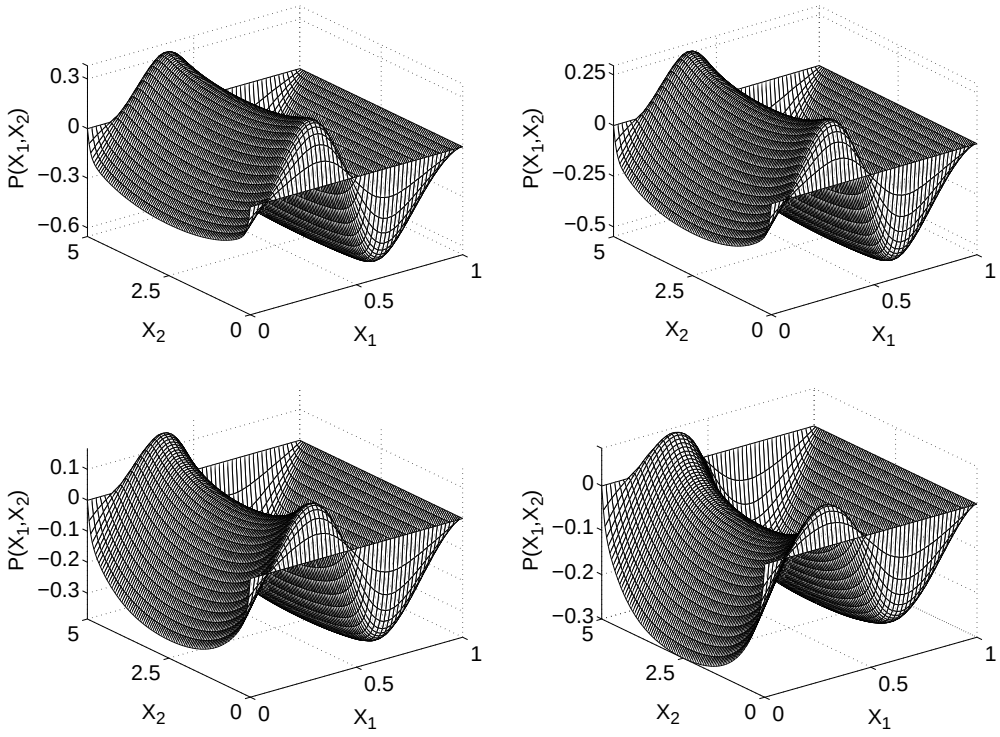

Fig. 16. Pressure distribution in a converging-diverging profile (from top left to bottom right): $r = 0.0$, $r = 0.2$, $r = 0.5$ and $r = 0.7$, obtained with $\widetilde{\mathrm{De}} = 1.3$ and $a = 0.8$

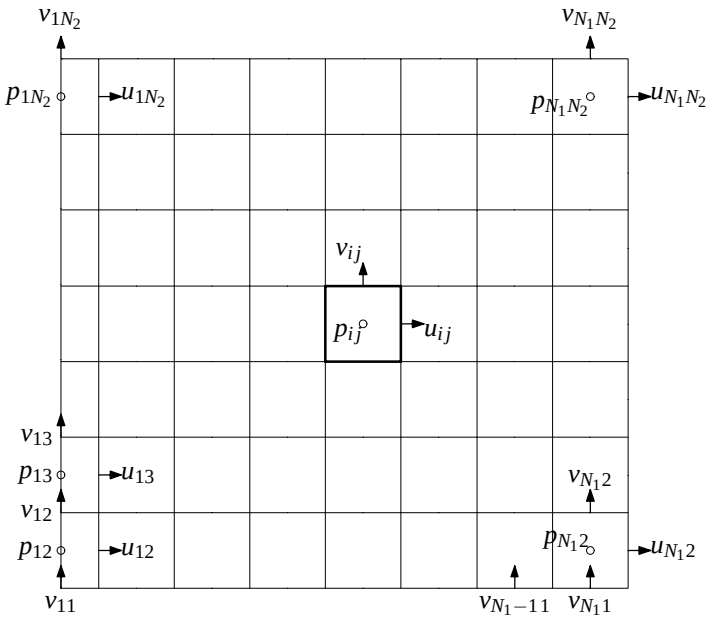

Fig. 17. Spatial discretisation and position of the unknowns p_{ij}, $\mathbf{u}_{ij} = (u_{ij}, v_{ij})$